Orbital torque of Cr-induced magnetization switching in perpendicularly magnetized Pt/Co/Pt/Cr heterostructures

Hongfei Xie(谢宏斐), Yuhan Chang(常宇晗), Xi Guo(郭玺), Jianrong Zhang(张健荣), Baoshan Cui(崔宝山), Yalu Zuo(左亚路)†, and Li Xi(席力)‡

Key Laboratory for Magnetism and Magnetic Materials of the Ministry of Education, Lanzhou University, Lanzhou 730000, *China*

(Received 16 September 2022; revised manuscript received 24 November 2022; accepted manuscript online 29 November 2022)

The spin–orbit torque via the spin Hall effect of heavy metals has shown promising prospect in driving the magnetization switching in spintronic devices due to the generated spin current from heavy metals. Recently, the 3d-light metals have been predicted the ability to generate orbital current and the associated orbital torques from the orbital Hall effect. However, few experiments have been carried out since it is quite hard to directly detect the orbital current-generated orbital torque. Here, we report an effective method to demonstrate the strong orbital torques in light metal Cr through a conversion process from orbital current to spin current by introducing the Pt interfacial layer in perpendicularly magnetized symmetric Pt/Co/Pt structures. A quite large and monotonically growth of orbital torque efficiency in Pt/Co/Pt/Cr with the increase of the thickness of Cr layer is obtained with the largest effective orbital torque efficiency around 2.6 Oe/(MA·cm^{-2}) (1 Oe = 79.5775 A·m^{-1}). The ability of orbital torque to drive the magnetization switching is also reported with the critical switching current density down to the order of 10^6 A·cm^{-2}. Our findings prove the efficiency for switching the magnetization from light metal Cr layers through the orbital Hall effect.

Keywords: spin Hall effect, orbital Hall effect, magnetization switching

PACS: 75.70.Tj, 75.60.–d, 77.80.Fm **DOI:** 10.1088/1674-1056/aca6d7

1. Introduction

Spin orbital torques (SOTs) in heavy metal/ferromagnetic bilayers attracted much attention due to its capability to efficiently drive the magnetization switching for magnetic memories and spin logic devices via the spin Hall effect of heavy metals and/or the interfacial Rashba effect.[1–5] So far, the promising materials for SOT-driven magnetization switching rely on heavy metals (HMs),[3,4] and 2d materials[6,7] and topological insulators[8–10] due to their strong spin current generating ability. The orbital torque from orbital current as the counterpart of spin orbital torque from spin current in materials was reported by Bernevig *et al*. in p-doped silicon,[11] 4d/5d transition metals,[12,13] and in 3d-transition light metals (LM) or CuO_x.[14,15] The theoretical prediction give rise to a comparable or even larger orbital torque efficiency than the conventional SOT in HM/FM, since the orbital Hall conductivity in light metals can be much larger than the corresponding spin Hall conductivity in heavy metals.[16] Thus, the orbital torque opens a new field for the research of high-efficiency spintronics devices using light metals rather than the expensive heavy metals, such as Pt. However, the conversion-coefficient from orbital current to spin current is too low to accurately detect the effective orbital torques in light metals.[17–19] To solve this problem, some experimental studies suggest a conversion mechanism from orbital current to spin current via heavy metals with strong spin orbit interaction in FM/HM/LM to obtain the strong orbital torque efficiency in light metals.[20,21]

In this work, the heavy metal Pt was used to convert the light metal Cr generated orbital current to spin current in perpendicular magnetized Ti/Pt/Co/Pt/Cr/Ti multilayers, in which the symmetric Pt/Co/Pt stacks was chosen for one hand to cancel the spin current generation from the bottom and up Pt layers due to its strong spin Hall effect,[3,4] and on other hand to ensure the interfacial perpendicular magnetic anisotropy on Pt/Co interface. Here, we choose light metal Cr due to the theoretically predicted large orbital Hall conductivity to generate orbital current.[15] The bottom and up Ti layers was used as the seed layer and protective layer, which eventually forms TiO_x protection layer for up Ti layers and shows negligible spin Hall effect.[22] To examine the production efficiency of the orbital torques in Cr, we perform the harmonic Hall voltage measurements to detect the effective fields in the Pt/Co/Pt/Cr multilayer. A monotonically evolution of the effective torque fields as a function of the Cr thickness is observed and ascribed to the orbital Hall effect (OHE) of Cr. Furthermore, we also found the magnetization switching induced by strong orbital torques in the Pt/Co/Pt/Cr multilayer, both of which demonstrate the ability of the orbital torque to tune the magnetization by means of the light metal Cr.

†Corresponding author. E-mail: zuoyl@lzu.edu.cn
‡Corresponding author. E-mail: xili@lzu.edu.cn

© 2023 Chinese Physical Society and IOP Publishing Ltd

2. Experimental methods

The Ti(3)/Pt(2)/Co(1)/Pt(2)/Cr(t_{Cr})/Ti(3) (thickness in unit nm) multilayers were deposited on corning glass substrates at room temperature by direct current magnetron sputtering with base pressure below 2.0×10^{-8} Torr (1 Torr = 1.33322×10^{2} Pa) and the thickness of Cr (t_{Cr}) is varied from 0.0 nm to 10.0 nm, setting by the sputtering time and the calibrated deposition rate. The multilayers were patterned to Hall bars with a dimension of 10 μm×200 μm by standard photolithography and Ar-ion etching techniques for magneto-transport measurement. The x-ray reflectivity spectra probed via grazing incidence measurements using Cu-$K\alpha$ radiation were used to characterize the thickness, density and roughness of each layer in multilayers. The t_{Cr} dependence of coercivity and perpendicular anisotropy fields of multilayers and the magnetic domain images were measured using a wide-field polar Kerr microscope working in the differential mode. Orbital torque efficiency was measured by harmonic Hall voltage measurements method using an analog–digital/digital–analog data acquisition card with the variation of the amplitude of sinusoidal current and keeping the frequency at 133 Hz.[23] All the above experiments were carried out at room temperature.

3. Results and discussion

To evaluate the influence of Cr capping layer on the structure parameters, including interfacial roughness, thickness and density of each layer, x-ray reflectivity (XRR) spectra were measured. Figure 1(a) shows the XRR spectrum examined by the high resolution PANalytical X'Pert^3 MRD diffractometer using Cu K_α (λ = 1.5406 Å) radiation. The XRR spectra were simulated by a GenX software with layer model of Ti/Pt/Co/Pt/Cr/Ti/TiO_x to obtain the thickness, roughness, density of each layer.[23,24] The obtained roughness and density of Co and Cr layer are shown in Fig. 1(b). As one can see the roughness of Co keeping around 3.5 Å with the increase of Cr layer thickness, indicating that the Cr layer does not show any influence on the underneath layer and the repeatability of the layered structure of our samples. While the roughness of Cr layer gradually increases from 4 Å to 8 Å with t_{Cr} increasing except the roughness of Cr layer is around 6.2 Å when t_{Cr} = 2 nm. We ascribed the anomalous point to the island structure of Cr atoms rather than the continually uniform layer structure when the thickness of Cr layer is too small, which is coincide with the growth mechanism of thin films by sputtering technique. Moreover, the density is around 8.9 g/cm^3 and 6.0 g/cm^3 for Co and Cr layers within the typical value of these two materials, respectively. Therefore, according to the information reflected by the XRR, we conclude that the prepared samples have high quality and clear interfaces. In principle, by sacrificing the Ti layer, the Cr layer will be protected from oxidation and deterioration due the capping Ti layer. To confirm our speculation, XPS was used to characterize the composition and valence state of Ti and Cr layers.

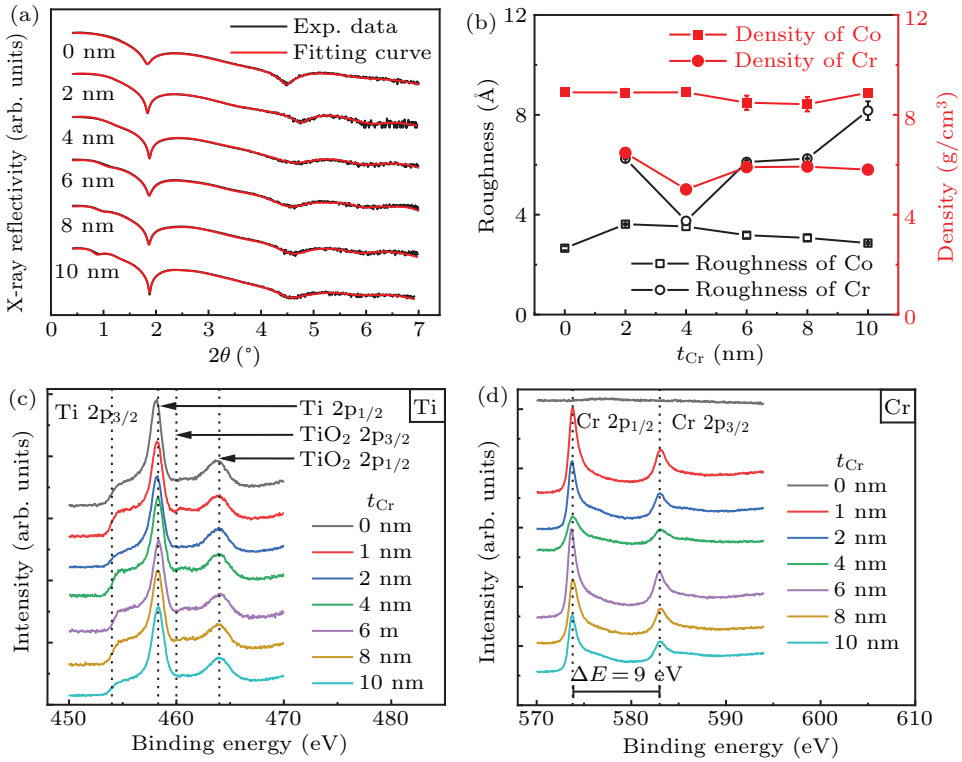


Fig. 1. The x-ray reflectivity spectra of Ti/Pt/Co/Pt/Cr/Ti samples with the variation of Cr thickness (a), the thickness-dependent interface roughness of Co/Pt and Cr/Ti, as well as the density of Co and Cr layers (b), the x-ray photoelectron spectra of Ti (c) and Cr (d) layers with the change of Cr thickness.

Figures 1(c) and 1(d) show the XPS spectra of Ti and Cr elements, respectively. The peak positions for $2p^{3/2}$ and $2p^{1/2}$ of metallic Ti are located at the binding energy of 454 eV and 458.3 eV, respectively, while the peak positions for $2p^{3/2}$ and $2p^{1/2}$ of TiO_2 are located at the binding energy of 460 eV and 464 eV, respectively. It indicates that there are metallic and oxides of Ti at the same time. For the Cr case, we can see that there are only metallic Cr $2p^{1/2}$ and Cr $2p^{3/2}$ peaks at the binding energy of 574 eV and 583 eV, respectively. The results revealed that the 3-nm-thick Ti layers is thick enough to protect Cr from the oxidation.

The magnetic properties of samples with the variation of t_{Cr} play important roles on electric current-induced magnetization switching, especially the nucleation field, the anisotropy, and the magnetic domain structures. We use the MOKE microscope to characterize the above parameters under the same magnetic field range and sweeping rate. The rectangular out-of-plane magnetized hysteresis loops in Fig. 2(a) indicate the existence of perpendicular magnetic anisotropy (PMA) of our samples. The nearly overlap of the hysteresis loops in Fig. 2(a) illuminates that the magnetizing process for all samples should be identical. To obtain perpendicular magnetic anisotropy field (H_k) of our samples, a large enough in-plane magnetic field was applied to saturate the magnetization in the plane. The thickness dependence of coercivity (H_c) and H_k is shown in Fig. 2(b). One can see that H_c and H_k are around 160 Oe and 3150 Oe, respectively (the error bars represent the standard deviation in multiple measurements), suggesting that the thickness of Cr layer has no obvious effect on the overall basic magnetic properties of the samples. Figures 2(c) and 2(d) show the exemplary MOKE pictures of the samples with $t_{Cr} = 0$ and 6 nm during domain nucleation, respectively. The results show that magnetic domains (white areas) in the two pictures have no obvious differences in the process of nucleation and expansion process, suggesting that Cr layers with different thicknesses have no effect on the nucleation process of magnetic domains. So far, we can conclude that the Ti/Pt/Co/Pt/Cr/Ti is an idea candidate to evaluate the orbit Hall effect of light metal Cr layers.

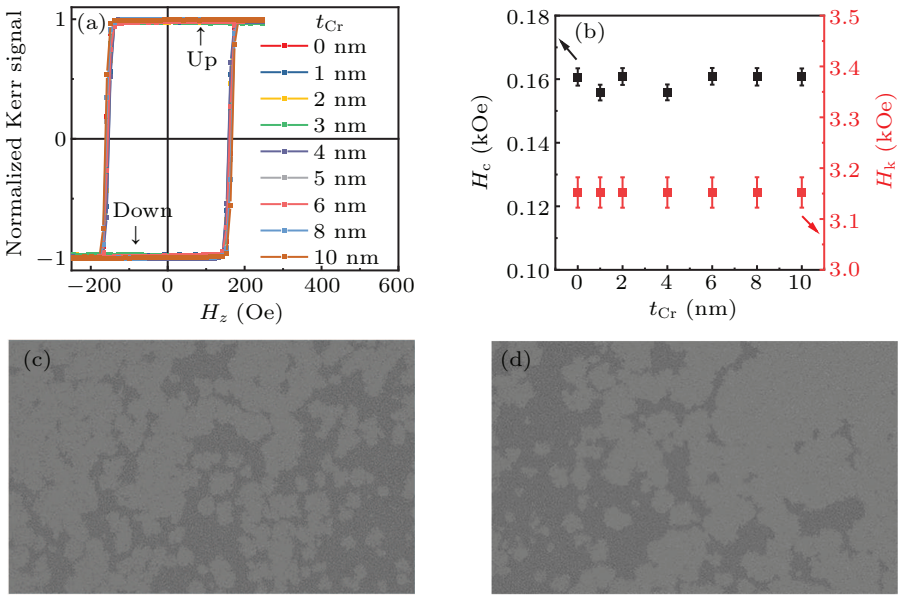


Fig. 2. The out-of-plane magnetized hysteresis loops for sample with the variation of the thickness of Cr layer (a), the thickness dependence of the coercivity (H_c) and the perpendicular magnetic anisotropic field (H_k) (b), and the magnetic domain structure for samples with $t_{Cr} = 0$ (c) and 6 nm (d).

To test the thickness-dependent spin orbital torque efficiency, a harmonic Hall voltage measurement method was employed. Figure 3(a) shows optical photographs of Hall bar and the measurement setup, in which a sinusoidal alternating current with amplitude I was passing along the x direction, the generated first (V^{ω}) and second ($V^{2\omega}$) harmonic Hall voltages were measured along the y direction. The damping-like and field-like spin orbital torques effective fields H_{DL} and H_{FL} were respectively calculated by Eq. (1) with the sweeping fields H_x and H_y along the x and y directions:[25]

$$H_{DL(FL)} = -2\frac{\partial V^{2\omega}}{\partial H_{x(y)}} \Big/ \frac{\partial^2 V^{\omega}}{\partial H_{x(y)}^2}. \quad (1)$$

Figures 3(b) and 3(c) show the variation trend of the first and second harmonic voltages of Ti/Pt/Co/Pt/Cr(6.0)/Ti sample when the field is swept in the x and y directions, respectively. The up- or down-magnetized states represent that the Hall bar was magnetized under a large out-of-plane field to obtain the nearly up-magnetized or down-magnetized single domains. The sweeping field range for H_x or H_y is small to ovoid breaking the up- or down-magnetized single domain states. The blue and green points in the figure represent the voltage value of the sample in the up and down magnetization states, respectively, and the red line is the corresponding fitting line. The obtained current dependent H_{DL} and H_{FL} are shown in Fig. 2(d). From the linear fitting the damping-like and field-

like spin orbital torque efficiency can be obtained and shown in Figs. 3(e) and 3(f). For the symmetrical Pt/Co/Pt structure, namely, the thickness of the Cr layer is 0 nm, the expected spin–orbit torque on the Co layer from top and bottom Pt layers should be cancelled out, however β_{DL} still has a none zero value of 0.78 Oe/(MA·cm^{-2}), indicating that such a symmetrical structure cannot completely offset the spin currents generated by the Pt layers on both sides of the Co layer, which should be related to the gentle different roughness caused by the growth environment of the two Pt layers as shown from the XRR fitting results. On this basis, a new spin current source was introduced into the system by the Cr layer and the possible origin includes the bulk spin Hall effect of the Cr layer, the spin current generated by the Cr–Pt interface and the spin current converted by the adjacent Pt layers from the orbital current generated by Cr layer. However the monotonically increase trend of $\beta_{\mathrm{DL/FL}}$ suggests that the spin current generated from Cr–Pt interface could be ruled out. Moreover, considering that the spin diffusion length of Pt is only 1.2 nm–1.4 nm,[26] which is smaller than the thickness of Pt layer in our sample, consequently, the spin current generated in the Cr layer cannot pass through the Pt layer and be absorbed by the Co layer. Thus, the monotonically increase of spin orbital torque efficiency with t_{Cr} should be explained by the giant conversion from orbital current of Cr layer to spin current via the Pt layer.[21]

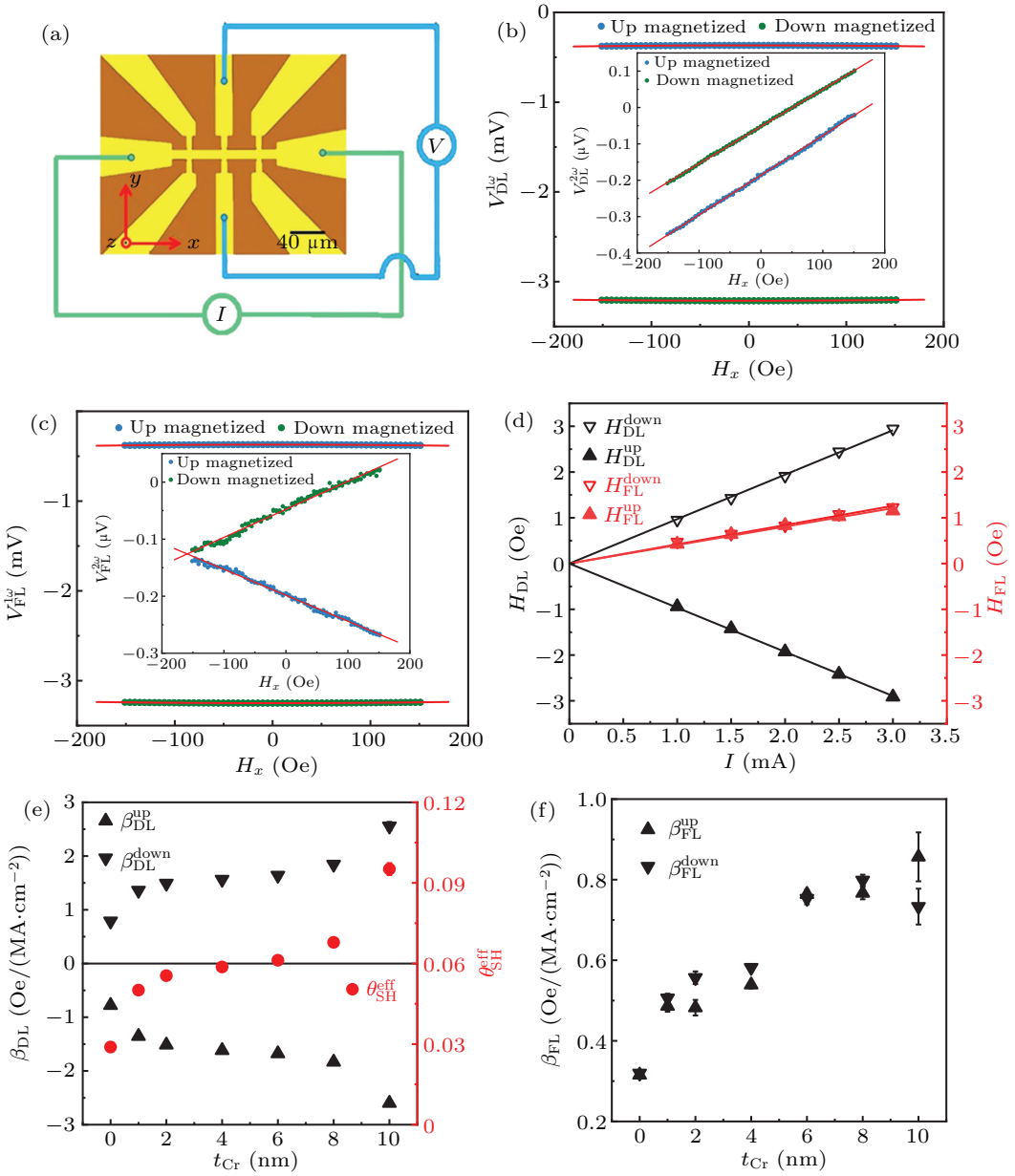


Fig. 3. The optical photographs of Hall bar and the established coordinate system for magneto-transport property measurement (a), the exemplary first harmonic Hall voltage with the sweeping of magnetic field along x axis for damping-like spin orbital torque efficiency measurement (b), the exemplary first harmonic Hall voltage with the sweeping of magnetic field along y axis for field-like spin orbital torque efficiency measurement (c), the obtained current-dependent damping-like and field-like spin orbital torque effective fields (d), the thickness-dependent damping-like (e) and field-like (f) spin orbital torque efficiencies. The insets in panels (b) and (c) show the field-dependent exemplary second harmonic Hall voltages. The thickness-dependent effective spin orbital Hall angle is also shown in panel (e).

Furthermore, then the thickness of Cr layer is 10 nm, the value of β_{DL} reaches 2.6 Oe/(MA·cm^{-2}), which is more than three times than that when the thickness of the Cr layer is 0 nm. In Fig. 3(f), the seminar variation trend of β_{FL} is also observed except the one order of magnitude smaller than that of β_{DL}, which is consistent with the spin Hall effect scenario. Thus, we can conclude that the spin current in our structure originates from the orbital current of Cr layer and passed through the Pt layer, rather than the spin current generated by the Pt layer via spin Hall effect. To see the thickness-dependent orbital Hall effect of Cr, the effective spin Hall angle were obtained from the damping-like torque efficiency by[27]

$$\theta_{SH/OH}^{eff} = \frac{2|e|M_s t_{FM}}{\hbar} \cdot \beta_{DL}, \tag{2}$$

where e and $\hbar$ are the electron charge and reduced Planck constant, respectively. M_s represents the saturation magnetization for the Co-layer with the thickness of t_{FM}. It can be seen a similar increase trend as the damping like torque efficiency. It should be mentioned that the second increase slope in damping and field like torque efficiency can be observed when $t_{Cr} \geq 6$ nm, which may be related to the phase transition of Cr layer as reported by Bose *et al.*[28] To compare the orbital Hall effect of Cr in this work to other light metals, we summarize the data of several light metals, such as, Cu, Ru, V, Zr, and Mn in Table 1. It can be seen that the Cr shows relatively larger orbital Hall conductivity and effective spin Hall angle in this work.

Table 1. The orbital Hall conductivity (σ_{OH}), spin Hall conductivity (σ_{SH}) and the effective spin Hall angles (θ_{SH}) for light metals at room temperature.

Element	σ_{OH} $(\hbar/e)(\Omega\cdot m)$	σ_{SH} $(\hbar/e)(\Omega\cdot m)$	θ_{SH}	Ref.
Cr	8200	−130	$(5.1\pm0.5)\times10^{-2}$	[29]
Cr	8831		$(9.5\pm0.2)\times10^{-2}$	this work
Cu	1200	30	$(3.2\pm0.3)\times10^{-3}$	[30]
Ru			3×10^{-1}	[31]
Zr	5300	−170	$-(3.0\pm0.2)\times10^{-2}$	[30,32]
V	5800	−90	$-(1.0\pm0.1)\times10^{-2}$	[30]
Mn	9200	−130	$-(1.9\pm0.1)\times10^{-1}$	[30]

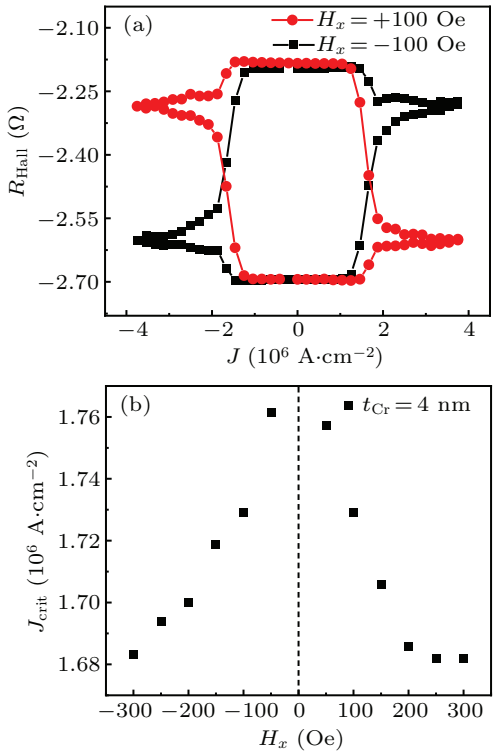


Fig. 4. (a) Orbit-torque-induced magnetization switching under fixed in-plane magnetic field $H_x = \pm100$ Oe. (b) Critical switching current density J_{crit} dependence on the magnetic field H_x.

Next, we focus on the orbit torque induced magnetization switching by current pulse. In the measurements, writing pulses with the width of 1 ms were injected along the current channel as shown in Fig. 3(a). After each writing pulses, the Hall voltage was measured by a small dc current of 1 mA. Meanwhile, an in-plane assisted magnetic field was applied to break the mirror symmetry. Figure 4(a) shows the current-driven magnetization switching curve under the assistant field $H_x = \pm100$ Oe. It is worth noting that the critical switching current density is as low as $\sim 1.72\times10^6$ A·cm^{-2}, which is comparable to the critical switching current density in the Pt and even in the topological insulator-based heterostructures,[3,4,10] implying an efficient mechanism of orbit torque switching from Cr layer. Furthermore, upon reversal of the applied in-plane field direction, the polarity of the current-induced switching loop also reverses, which is consistent with the spin orbital torque switching scenario. The scenario was also confirmed by a smaller H_x, the larger critical switching current density as shown in Fig. 2(b). Thus, thanks for the efficient conversion mechanism of Pt from the orbital current to spin current, a rather energy efficient magnetization switching is achieved using the orbital Hall effect of light metal Cr.

4. Conclusion

In conclusion, we provided an effective method to directly detect the orbit torque by converting the orbital current in light metal Cr into spin current via a Pt insertion layer in a perpendicularly magnetized symmetric Pt/Co/Pt/Cr structure.

The harmonic measurements results demonstrated that the orbital torque efficiency in Pt/Co/Pt/Cr increases with the Cr layer thickness increasing, while the orbit torque can be used to achieve the perpendicular magnetization switching. Our results provide an effective pathway to characterize the orbit torque and achieve the perpendicular magnetization switching, advancing the practical applications of orbit torque systems in data memory, logic, and computing devices.

Acknowledgements

Project supported by the National Natural Science Foundation of China (Grant Nos. 91963201 and 51671098), the 111 Project (Grant No. B20063), the Program for Changjiang Scholars and Innovative Research Team in University PCSIRT (Grant No. IRT16R35), and the Natural Science Foundation of Gansu Province, China (Grant No. 22JR5RA474).

References

[1] Kato Y K, Myers R C, Gossard A C and Awschalom D D 2004 *Science* **306** 1910
[2] Murakami S 2005 *Advances in Solid State Physics* **45** (Berlin, Heidelberg: Springer-Verlag) p. 209
[3] Sinova J, Valenzuela S O, Wunderlich J, Back C H and Jungwirth T 2015 *Rev. Mod. Phys.* **87** 1213
[4] Manchon A, Železný J, Miron I M, Jungwirth T, Sinova J, Thiaville A, Garello K and Gambardella P 2019 *Rev. Mod. Phys.* **91** 035004
[5] Hoffmann A 2013 *IEEE Trans. Magn.* **49** 5172
[6] Husain S, Gupta R, Kumar A, Kumar P, Behera N, Brucas R, Chaudhary S and Svedlindh P 2020 *Appl. Phys. Rev.* **7** 041312
[7] Chen Q, Lv W, Li S, Lv W, Cai J, Zhu Y, Wang J, Li R, Zhang B and Zeng Z 2021 *Chin. Phys. B* **30** 097506
[8] Mellnik A R, Lee J S, Richardella A, Grab J L, Mintun P J, Fischer M H, Vaezi A, Manchon A, Kim E A, Samarth N and Ralph D C 2014 *Nature* **511** 449
[9] Wu H, Zhang P, Deng P, Lan Q, Pan Q, Seyed A R, Che X, Huang L, Dai B, Wong K, Han X and Wang K L 2019 *Phys. Rev. Lett.* **123** 207205
[10] Zhang X, Zhang J, Zhai Y, Bai Q, Chang M, Yan Z, Zuo Y and Xi L 2021 *Phys. Status Solidi RRL* **15** 2100327
[11] Bernevig B A, Hughes T L and Zhang S C 2005 *Phys. Rev. Lett.* **95** 066601
[12] Go D, Jo D, Kim C and Lee H W 2018 *Phys. Rev. Lett.* **121** 086602
[13] Kontani H, Tanaka T, Hirashima D S, Yamada K and Inoue J 2009 *Phys. Rev. Lett.* **102** 016601
[14] Go D, Jo D, Gao T, Ando K, Blügel S, Lee H W and Mokrousov Y 2021 *Phys. Rev. B* **103** L121113
[15] Jo D, Go D and Lee H W 2018 *Phys. Rev. B* **98** 214405
[16] Zheng Z C, Guo Q X, Jo D, Go D, Wang L H, Chen H C, Yin W, Wang X M, Yu G H, He W, Lee H W, Teng J and Zhu T 2020 *Phys. Rev. Res.* **2** 013127
[17] Lee D, Go D, Park H J, Jeong W, Ko H W, Yun D, Jo D, Lee S, Go G, Oh J H, Kim K J, Park B G, Min B C, Koo H C, Lee H W, Lee O and Lee K J 2021 *Nat. Commun.* **12** 6710
[18] Ding S, Liang Z, Go D, Yun C, Xue M, Liu Z, Becker S, Yang W, Du H, Wang C, Yang Y, Jakob G, Kläui M, Mokrousov Y and Yang J 2022 *Phys. Rev. Lett.* **128** 067201
[19] Go D and Lee H W 2020 *Phys. Rev. Res.* **2** 013177
[20] Ding S, Ross A, Go D, Baldrati L, Ren Z, Freimuth F, Becker S, Kammerbauer F, Yang J, Jakob G, Mokrousov Y and Kläui M 2020 *Phys. Rev. Lett.* **125** 177201
[21] Lee S, Kang M G, Go D, Kim D, Kang J H, Lee T, Lee G H, Kang J, Lee N J, Mokrousov Y, Kim S, Kim K J, Lee K J and Park B G 2021 *Commun. Phys.* **4** 234
[22] Baek S C, Amin V P, Oh Y W, Go G, Lee S J, Lee G H, Kim K J, Stiles M D, Park B G and Lee K J 2018 *Nat. Mater.* **17** 509
[23] Yun J, Bai Q, Yan Z, Chang M, Mao J, Zuo Y, Yang D, Xi L and Xue D 2020 *Adv. Funct. Mater.* **30** 1909092
[24] Björck M and Andersson G 2007 *J. Appl. Crystallogr.* **40** 1174
[25] Kim J, Sinha J, Hayashi M, Yamanouchi M, Fukami S, Suzuki T, Mitani S and Ohno H 2013 *Nat. Mater.* **12** 240
[26] Sagasta E, Omori Y, Isasa M, Gradhand M, Hueso Luis E, Niimi Y, Otani Y and Casanova F 2016 *Phys. Rev. B* **94** 060412
[27] Althammer M, Meyer S, Nakayama H, Schreier M, Altmannshofer S, Weiler M, Huebl H, Geprägs S, Opel M, Gross R, Meier D, Klewe C, Kuschel T, Schmalhorst J M, Reiss G, Shen L, Gupta A, Chen Y T, Bauer G E W, Saitoh E and Goennenwein S T B 2013 *Phys. Rev. B* **87** 224401
[28] Bose A, Singh H, Kushwaha V K, Bhuktare S, Dutta S and Tulapurkar A A 2018 *Phys. Rev. Appl.* **9** 014022
[29] Sala G and Gambardella P 2022 *Phys. Rev. Res.* **4** 033037
[30] Du C, Wang H, Yang F and Hammel P C 2014 *Phys. Rev. B* **90** 140407
[31] Liao L, Xue F, Han L, Kim J, Zhang R, Li L, Liu J, Kou X, Song C, Pan F and Otani Y 2022 *Phys. Rev. B* **105** 104434
[32] Zheng Z C, Guo Q X, Jo D, Go D, Wang L H, Chen H C, Yin W, Wang X M, Yu G H, He W, Lee H W, Teng J and Zhu T 2020 *Phys. Rev. Res.* **2** 013127